Journal of Advanced Research 34 (2021) 29–41

Contents lists available at ScienceDirect

Journal of Advanced Research

journal homepage: www.elsevier.com/locate/jare

A Tumor-Specific Ferric-Coordinated Epigallocatechin-3-gallate cascade nanoreactor for glioblastoma therapy

Min Mu [a,1], Haifeng Chen [a,1], Rangrang Fan [a,1], Yuelong Wang [a], Xin Tang [a], Lan Mei [a], Na Zhao [b], Bingwen Zou [a], Aiping Tong [a], Jianguo Xu [a], Bo Han [b], Gang Guo [a,*]

[a] State Key Laboratory of Biotherapy and Cancer Center, and Department of Neurosurgery, West China Hospital, Sichuan University, and Collaborative Innovation Center for Biotherapy, Chengdu, 610041, China
[b] School of Pharmacy, Shihezi University, and Key Laboratory of Xinjiang Phytomedicine Resource and Utilization, Ministry of Education, Shihezi, 832002, China

GRAPHICAL ABSTRACT

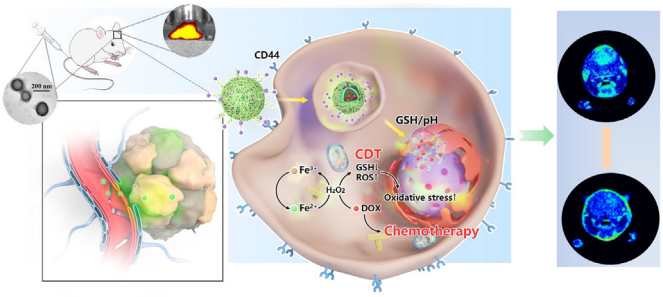

ARTICLE INFO

Article history:
Received 13 April 2021
Revised 21 July 2021
Accepted 28 July 2021
Available online 30 July 2021

Keywords:
Glioblastoma
Epigallocatechin-3-gallate
Chemodynamic therapy
Fenton reaction
Acid/glutathione responsiveness

ABSTRACT

Introduction: Numerous options for treatment of glioblastoma have been explored; however, single-drug therapies and poor targeting have failed to provide effective drugs. Chemotherapy has significant antitumor effect, but the efficacy of single-drug therapies in the clinic is limited over a long period of time. Thus, novel therapeutic approaches are necessary to address these critical issues.
Objectives: The present study, we investigated a tumor-specific metal-tea polyphenol-based cascade nanoreactor for chemodynamic therapy-enhanced chemotherapy.
Methods: HA-EGCG was synthesized for the first time by introducing epigallocatechin-3-gallate (EGCG) into the skeleton of hyaluronic acid (HA) with reducible disulfide bonds. A rapid and green method was developed to fabricate the metal-tea polyphenol networks (MTP) with an HA-EGCG coating (DOX@MTP/HA-EGCG) based on Fe^{3+} and EGCG for targeted delivery of doxorubicin hydrochloride (DOX). GL261 cells were used to evaluate the antitumor efficacy of the DOX@MTP/HA-EGCG nanoreactor *in vitro* and *in vivo*.
Results: DOX@MTP/HA-EGCG nanoreactors were able to disassemble, resulting in escape of their components from lysosomes and precise release of DOX, Fe^{3+}, and EGCG in the tumor cells. HA-EGCG depleted glutathione to amplify oxidative stress and enhance chemodynamic therapy. The results of *in vivo* experiments suggested that DOX@MTP/HA-EGCG specifically accumulates at the CD44-overexpressing GL261 tumor sites and that sustained release of DOX and Fe^{3+} induced a distinct therapeutic outcome.

Peer review under responsibility of Cairo University.
* Corresponding author at: No.17 Section 3, South Renmin Road, Wuhou District, Chengdu, Sichuan province, China.
E-mail address: guogang@scu.edu.cn (G. Guo).
[1] These authors contributed equally to this work.

https://doi.org/10.1016/j.jare.2021.07.010
2090-1232/

Conclusions: The findings suggested the developed nanoreactor has promising potential as a future GL261 glioblastoma therapy.

Introduction

Glioblastoma is a malignant tumor with a median survival of approximately 15–17 months after the treatments with surgical resection, radiotherapy, and chemotherapy [1–3]. Considerable efforts have been spent to explore new treatment approaches, including photodynamic therapy, photothermal therapy, and immunotherapy; however, chemotherapy is the major modality clinically used for cancer treatment. The blood–brain barrier (BBB) and poor targeting limit the distribution of the drugs in glioblastoma. BBB, is the natural defense system of the brain that protects against the entry of foreign bodies, and prevents penetration of beneficial drugs in the brain [4]. Thus, glioblastoma treatment requires the penetration through the BBB and improved targeting.

Reactive oxygen species (ROS)-based therapy works against tumors because of the strong oxidizing properties of ROS [5–7]. Chemodynamic therapy (CDT) realized through the Fenton reaction has become a new "green" selective and specific therapy. Notably, CDT combines the tumor microenvironment with Fenton or Fenton-like reactions to induce cell death and has potential for clinical translation. During CDT, a high level of intratumoral H_2O_2 is converted to ROS, including hydroxyl radicals (·OH), in the presence of catalysts (e.g., Cr, Fe, Mn, and Cu) [8–10]. However, a high level of glutathione (GSH) in the tumor microenvironment represents a barrier against ·OH. Therefore, upregulation of ROS and downregulation of GSH levels in the tumors are considerable strategies to amplify oxidative stress and thus enhance the efficacy of CDT [11–13]. Catalytic activity of Fe^{3+} in the Fenton reaction is lower than that of Fe^{2+} [14,15], which inspired us to introduce an Fe^{2+}-supply-regeneration system into a cancer context to address poor efficacy of the Fenton reaction [16–18]. Naturally derived polyphenol epigallocatechin-3-gallate (EGCG) is an acid-activated reductant that can reduce Fe^{3+} to Fe^{2+} and thus improve the efficiency of the Fenton reaction in acidic tumor microenvironment [18,19]. Metal polyphenol networks (MTP) involve coordination of polyphenols and metals and have received increasing attention in nanomedicine and biotechnology [15,19].

CD44 is a cell-surface glycoprotein closely related to the proliferation, migration, adhesion and differentiation of cells and is overexpressed on various tumor cells, including colon cancer, breast cancer, and glioblastoma cells [20,21]. Hyaluronic acid (HA) is a biocompatible natural polysaccharide with low immunogenicity that has strong affinity for the CD44 receptor. HA acts as a targeting moiety for targeted therapy to enter tumor cells predominantly via a receptor-mediated mechanism to increase drug levels in a lesion area. Recent reports demonstrated that EGCG can induce the disruption of tight junctions and BBB [22–25]; thus, we were the first to introduce the smart carrier material HA-S-S-EGCG (HA-EGCG) comprising HA and EGCG for glioblastoma therapy. HA-EGCG is a pilot compound with dual functions, including the depletion of GSH due to breaking of disulfide bonds to expand oxidative stress and targeting the CD44 receptor overexpressed on the surface of the tumor cells [26].

The present study constructed MTP to deliver DOX based on EGCG and Fe^{3+} to form DOX@MTP for glioblastoma therapy (scheme 1). DOX@MTP were formed by coordination of EGCG and Fe^{3+}. The DOX@MTP/HA-EGCG nanoreactor was produced after introduction of HA-EGCG via self-assembly. DOX@MTP/HA-EGCG was designed based on the following considerations. (I) The nanoreactor can penetrate through the BBB due to the effect of EGCG to enhance the permeability and retention (EPR) effect. (II) HA in DOX@MTP/HA-EGCG serves as a targeting ligand, which improves selective accumulation of the molecules in CD44-overexpressing tumor tissues. (III) MTP dissociates to release DOX, EGCG, and Fe^{3+} in acidic and GSH-containing environments of the tumor cells. EGCG reduces Fe^{3+} to continuously supply Fe^{2+} to convert H_2O_2 to ·OH via the Fenton reaction to enhance chemotherapy. (IV) The disulfide bonds of the HA-EGCG carrier induce a decrease in the elevated GSH levels in the tumor cells to amplify oxidative stress. These multiple mechanisms can overcome natural BBB, improve selective tumor targeting, and increase the therapeutic effects of CDT-enhanced chemotherapy for glioblastoma.

Experimental section

Materials

Hyaluronic acid (HA, 97%) (MW ≈ 9000 Da) was purchased from Shandong Freda Biopharmaceutical Co., Ltd. Cysteamine dihydrochloride (>97%), 4-(4,6-dimethoxy-1,3,5-triazin-2-yl)-4-methyl morpholinium chloride (DMTMM, 97%), and glutathione (GSH, 98%) were purchased from Aladdin (Shanghai, China). Iron chloride hexahydrate ($FeCl_3{\cdot}6H_2O$, 99%) was purchased from Sigma-Aldrich. Epigallocatechin-3-gallate (EGCG, 95%) and Doxorubicin (DOX, >98%) were purchased from Meilun Biotechnology Co., Ltd. Annexin V-fluorescein isothiocyanate (FITC)/7-aminoactinomycin D (7AAD), 4′,6-diamidino-2-phenylindole (DAPI), and lysosomal probes were purchased from Beyotime Biotechnology (Shanghai). Antibodies against CD44, CD31, Ki67, β-actin, and caspase 3 were purchased from Abcam (Massachusetts, USA).

Synthesis of HA-EGCG

DMTMM is a triazine-based condensing reagent that promotes the coupling reaction between the $-NH_2$ group of cysteamine and –COOH groups of HA to obtain HA-S-S-NH_2. Then, HA-S-S-NH_2 was incubated with an excess of EGCG under weakly alkaline conditions. An *ortho*-quinone structure is formed at the EGCG backbone at weakly alkaline pH due to autoxidation of EGCG [17]. Finally, HA-EGCG was synthesized via nucleophilic reaction between HA-S-S-NH_2 and the *ortho*-quinone moiety of EGCG.

Preparation and characterization of DOX@MTP, DOX/HA-EGCG, and DOX@MTP/HA-EGCG

DOX@MTP/HA-EGCG was prepared according to a previous report with some modifications [19,27]. Briefly, 200 μL of $FeCl_3$ solution (0.27 mg/mL) was added to 1 mL of distilled water and 400 μg of DOX solution, and 300 μL of EGCG solution (2 mg/mL) was added dropwise to the mixture under stirring. After the formation of DOX@MTP, HA-EGCG solution (10 mg/mL) was added and the mixture was incubated for 1 h and centrifuged to remove free DOX and insoluble materials to obtain DOX@MTP/HA-EGCG nanoreactors. An equivalent volume of water was used instead of DOX to prepare MTP and MTP/HA-EGCG. DOX/HA-EGCG was formed by self-assembly based on DOX and HA-EGCG. DOX solu-

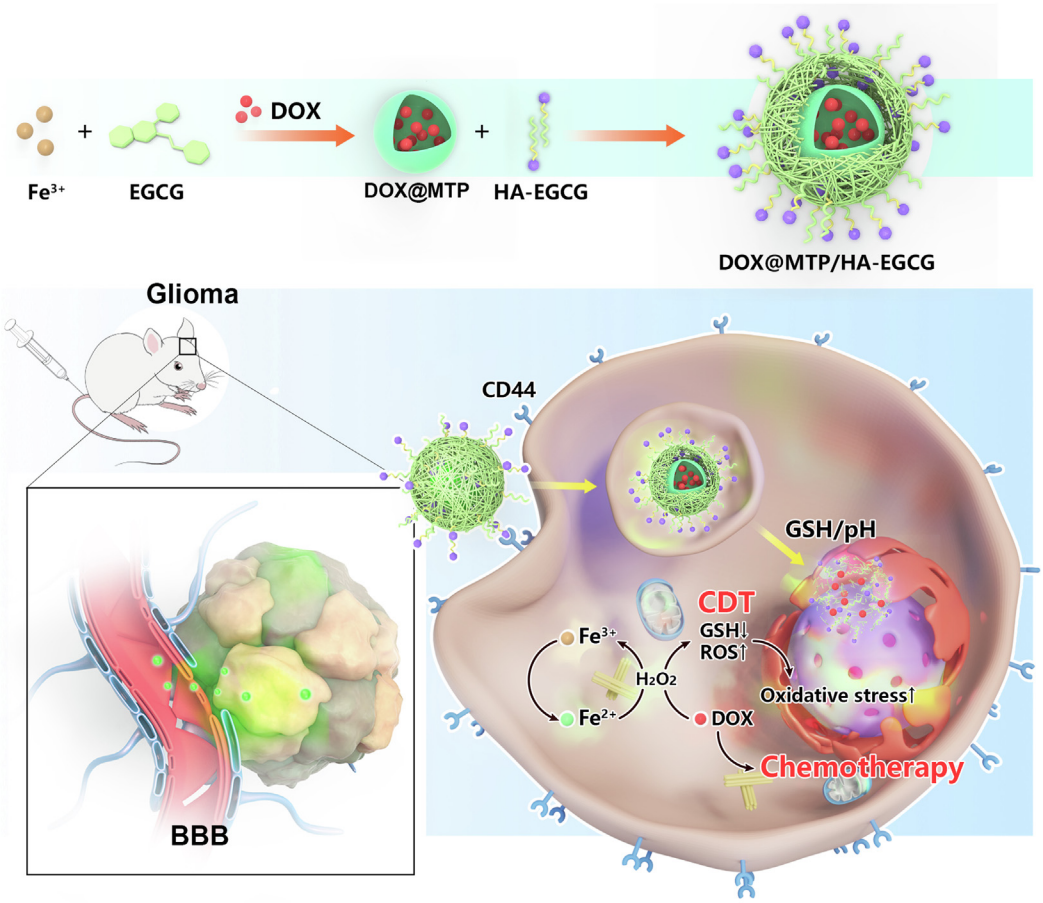

Scheme 1. Schematic illustration of DOX@MTP/HA-EGCG nanoreactor. The nanoreactor penetrate the blood–brain barrier and target glioblastoma therapy via CDT and chemotherapy.

tion was added to HA-EGCG solution under magnetic stirring for 1 h to obtain DOX/HA-EGCG.

The sizes of the DOX@MTP, DOX/HA-EGCG, and DOX@MTP/HA-EGCG nanoreactors were measured by dynamic light scattering (DLS) (Nano-ZS 90; Malvern, UK). Transmission electron microscopy (TEM; H-6009IV; Hitachi, Japan) was used to assess the morphology of the nanoreactors. Phosphotungstic acid (2% (w/w)) was used to stain the nanoreactors for 5 min before observation. Atomic force microscopy (AFM) (Bruker, MultiMode) was applied to evaluate the surface morphology of the nanoreactor.

Evaluation of ·OH generation

The ·OH generation ability of MTP and MTP/HA-EGCG in various buffers was measured using methylene blue (MB) as an indicator [13]. Briefly, MTP and MTP/HA-EGCG (200 μM of Fe^{3+}) were added in phosphate-buffered saline (PBS) (pH = 5.4 and 7.4) containing H_2O_2 (10 mM) and MB (25 μg/mL). After incubation for 30 min at 37 °C, the absorbance spectra were recorded by UV–vis spectroscopy.

Mechanism of targeting and endocytosis of DOX@MTP/HA-EGCG

GL261 cells were supplied by American Type Culture Collection. To determine the targeting ability of HA, GL261 cells were incubated with free HA (10 mg/mL) for 1 h before treatment with DOX@MTP/HA-EGCG [28]. Subsequently, the culture medium was removed. The cells were treated with fresh medium containing the DOX@MTP/HA-EGCG nanoreactors (0.2 μg/mL of DOX) for 4 h and assayed by confocal laser scanning microscopy (CLSM) and flow cytometry.

To investigate the possible endocytosis mechanisms, the various endocytosis inhibitors were introduced [29]. Firstly, GL261 cells were seeded into 12 and 24-well plates and cultured overnight. Then, the cells were preincubated with various inhibitors of endocytosis, including free HA (10 mg/mL), methyl-β-cyclodextrin (M-β-CD) (2 μM), dynasore (100 μM), chlorpromazine (20 μM) and 5-(N-ethyl-N-isopropyl) amiloride (EIPA) (100 μM). After 2 h of preincubation, the inhibitors were removed, and GL261 cells were incubated in serum-free medium for another 2 h. Finally, the cells in a 12-well plate were collected for analysis by flow cytometry, and the cells in a 24-well plate were imaged by CLSM.

In vitro BBB model study

To establish an *in vitro* BBB model, brain-derived endothelial cells.3 (bEnd.3) cells were seeded into 24-well cell culture inserts at a density of 4×10^4 per well to determine if transendothelial electric resistance (TEER) was greater or lower than 300 Ω [26]. GL261 cells were seeded into another 24-well plate with a cover glass and then cocultured with bEnd.3 monolayers for one day. The bEnd.3 cell monolayer was treated with DOX, DOX@MTP, DOX/HA-EGCG, and DOX@MTP/HA-EGCG solutions (0.12 μg/mL of DOX). Finally, bEnd.3 and GL261 cells were imaged by CLSM after 4 h of treatment.

Ethics statement

All animal experiments were approved by the Animal Ethics Committee of West China Hospital of Sichuan University and were performed in accordance with the Guidelines for Care and Use of Laboratory Animals of Sichuan University (20211055A).

In vivo tumor model

Female C57BL/6 mice (7–8 weeks) were purchased from Beijing HFK Bioscience Co., Ltd. GL261-luc glioblastoma-bearing C57BL/6 mice were generated as described in our previous report. C57BL/6 mice were anesthetized and fixed, and GL261-luc cells (5×10^4 cells suspended in 5 μL of serum-free DMEM) were implanted into the right striatum of C57BL/6 mice using a 10-μL Hamilton syringe. GL261 glioblastoma-bearing mice were randomly divided into six groups (n = 5) 10 days after the implantation.

To detect biodistribution of the nanoreactors, we replaced DOX with rhodamine B (RB, a fluorescent dye) [30]. Mice were intravenously injected with free RB, RB@MTP, RB/HA-EGCG, and RB@MTP/HA-EGCG. The RB dose was 10 mg/kg. All mice were examined 2, 6, 10, 12, and 24 h after the injection using a PerkinElmer IVIS instrument with excitation at 520 nm and emission at 620 nm. Mice were sacrificed, and the brain and major organs (heart, liver, spleen, lung and kidney) were harvested 24 h later for *ex vivo* imaging of RB.

In vivo tumor therapy

GL261-luc glioblastoma-bearing C57BL/6 mice were established in our previous literature. GL261 glioblastoma-bearing mice were randomly divided into six groups (n = 5) after implantation for 10 days. The six groups of GL261-luc glioblastoma-bearing C57BL/6 mice were intravenously injected four times with various formulations every two days, including NS, MTP/HA-EGCG (3.5 mg/kg of Fe^{3+}, DOX (2.5 mg/kg of DOX), DOX@MTP (3.5 mg/kg of Fe^{3+}, 2.5 mg/kg of DOX), DOX/HA-EGCG (2.5 mg/kg of DOX, 15 mg/kg of HA-EGCG), and DOX@MTP/HA-EGCG (3.5 mg/kg of Fe^{3+}, 2.5 mg/kg of DOX, 15 mg/kg of HA-EGCG) and the survival time and body weights were recorded. For *in vivo* bioluminescence analysis of the tumors, GL261-luc glioblastoma-bearing mice were administered D-luciferin potassium salt for 10 min and then anesthetized with isoflurane. Mice were imaged to evaluate the therapeutic efficiency 10, 17, and 24 days after the implantation.

Statistical analysis

All experiments were performed in triplicate, and the data are presented as the mean ± standard deviation (SD). All data analyses were carried out using GraphPad 7.0 software.

Results and discussion

Synthesis and characterization of HA-EGCG

The scheme of HA-EGCG synthesis is illustrated in Figure S1. Proton nuclear magnetic resonance (^{1}H NMR) spectroscopy was used to characterize the structure of HA-EGCG (Figure S2). The proton signals of the B ring (6'') were shifted to 6.65 ppm compared with the signals of unmodified EGCG (6.5 ppm). The relative peak area of the B ring was lower than that of the D ring, indicating that a single proton of the B ring disappeared after the modification [31,32]. HA-EGCG had an additional UV absorption peak corresponding to EGCG, which was not detected in HA (Figure S3). The peak displayed a weak redshift compared with the peak in EGCG [18,33]. The results of ^{1}H NMR and UV spectral analysis indicated that HA-EGCG carrier was successfully prepared. Additionally, we evaluated the biocompatibility of the HA-EGCG preparation (Figure S4). At an EGCG concentration of 1000 μg/mL, the hemolysis rates induced by EGCG and HA-EGCG were 39.8 ± 0.2% and 4.7 ± 0.1%, respectively. Modification with HA, reduced hemolysis induced by EGCG and improved the biosafety of EGCG.

Preparation and characterization of DOX@MTP, DOX/HA-EGCG, and DOX@MTP/HA-EGCG

The galloyl and catechol groups of EGCG provide multivalent chelating sites with acid responsiveness to coordinate with many metals. Thus, DOX@MTP was prepared using a self-deposited network upon chelation of EGCG with Fe^{3+} in the presence of DOX. MTP is characterized by high biosafety, versatile functionalization and pH-responsiveness; hence, DOX@MTP disintegrated in an acidic environment to release DOX, Fe^{3+}, and EGCG [34,35]. HA-EGCG was introduced to promote active targeting and amplify oxidative stress induced by DOX@MTP. Hydrogen bonding, π-π stacking, and hydrophobic interactions are responsible for EGCG binding to many compounds, including DNA and proteins [31,36,37]. Thus, we presumed that prepared DOX@MTP co-incubated with HA-EGCG for 1 h formed DOX@MTP/HA-EGCG via self-assembly. The nanoreactor was formed by a simple and green method that did not involve organic reagents. To further evaluate CDT-enhanced chemotherapy, DOX/HA-EGCG was prepared from HA-EGCG and DOX and was formed due to hydrogen bonds and π-π stacking; this preparation was used as a control [37].

The sizes of the DOX@MTP, DOX/HA-EGCG, and DOX@MTP/HA-EGCG nanoreactors were determined by DLS (Fig. 1A). In addition, the morphologies of the DOX@MTP, DOX/HA-EGCG, and DOX@MTP/HA-EGCG nanoreactors were also imaged by TEM (Fig. 1B). All of them had spherical shapes and monodispersity. The size observed by TEM was smaller than that measured by DLS mainly due to the shrinkage of the nanoreactors. After introduction of HA-EGCG, DOX@MTP/HA-EGCG displayed a uniform spherical morphology with a core–shell structure, presented an increased diameter (about 40 nm), and had a smooth surface. But the morphology of DOX@MTP/HA-EGCG nanoreactors changed after incubation in the presence of 10 mM GSH, implying the dissociation of the nanoreactor, the cleavage of disulfide bonds and aggregation formation. As shown in Table S1, the zeta potential of DOX@MTP/HA-EGCG shifted from + 10.6 ± 1.2 to −26.4 ± 3.3 mV because of successful addition of negatively charged HA-EGCG. Atomic force microscopy (AFM) was applied to evaluate the surface morphology of DOX@MTP, DOX/HA-EGCG, and DOX@MTP/HA-EGCG (Figure S5). AFM images showed a spherical shape and smooth surface of DOX/HA-EGCG and DOX@MTP/HA-EGCG. But for DOX@MTP, the surface morphology was irregular and similar to spherical. The results were consistent with those of TEM.

The stability of DOX@MTP, DOX/HA-EGCG, and DOX@MTP/HA-EGCG was determined by DLS (Figure S6). The sizes of the nanoreactors were not significantly changed after 7 days in a 25 °C thermostat, suggesting that the nanoreactors have great storage stability. The thermal properties of DOX@MTP, DOX/HA-EGCG, and MTP/HA-EGCG were examined by TGA. The TGA and DTG profiles within temperature range of 30–600 °C are shown in Figure S7. The results showed that the weight loss observed below 150 °C was caused by water evaporation [38]. The most weight loss in the range of 200–600 °C could be attributed to the decomposition of DOX and HA-EGCG layer in DOX/HA-EGCG and MTP/HA-EGCG [39]. In the TGA curve of DOX@MTP, 13.7% mass loss between 200 and 280 °C might be caused by DOX [39,40]. The decomposition of DOX@MTP occurs between 300 and 500 °C with a weight loss approximate 25% which might be attributed to

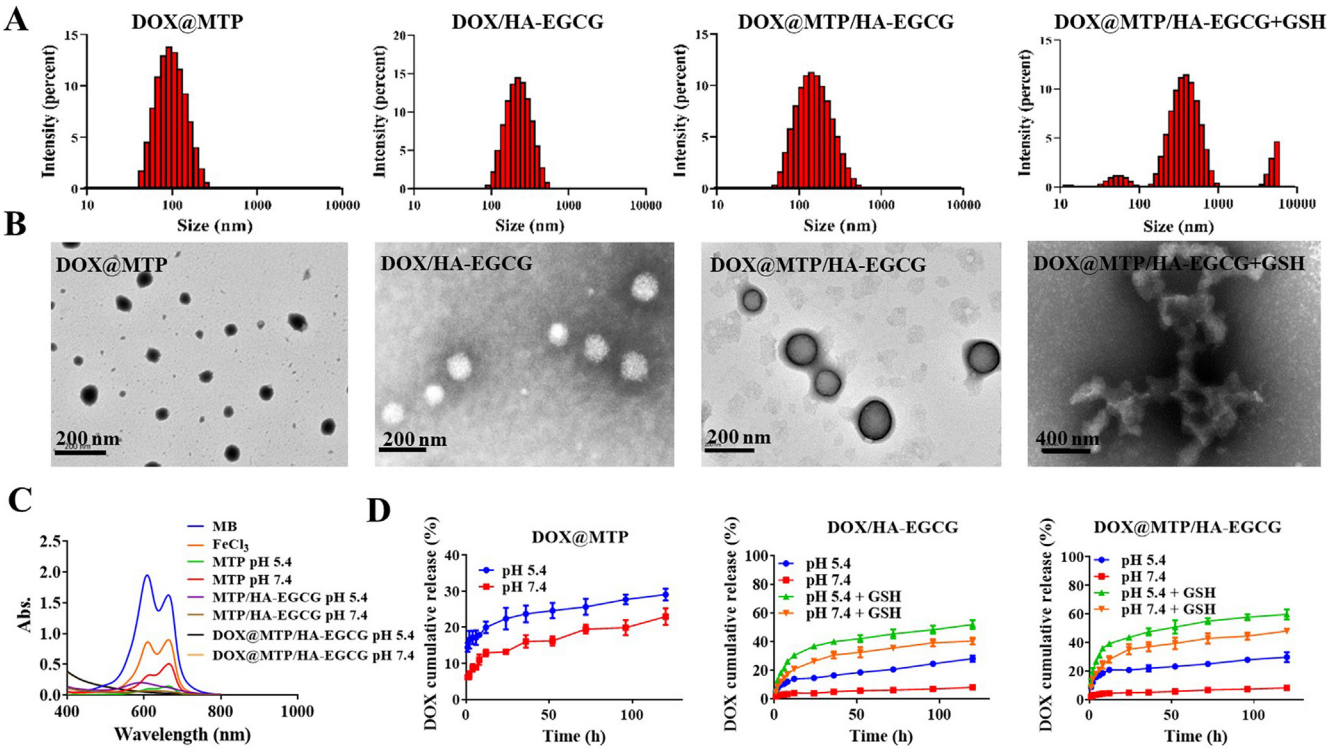

Fig. 1. Characterization of DOX@MTP/HA-EGCG NPs. DLS (A) and TEM (B) images of DOX@MTP, DOX/HA-EGCG, DOX@MTP/HA-EGCG, and DOX@MTP/HA-EGCG + 10 mM GSH. (C) UV–vis spectra of MB solution after reaction with H_2O_2, $FeCl_3$ + H_2O_2, MTP + H_2O_2 (pH 5.4 and 7.4), MTP/HA-EGCG + H_2O_2, and DOX@MTP/HA-EGCG + H_2O_2 (pH 5.4 and 7.4). The reaction time was 30 min. (D) In vitro drug release profile of DOX in DOX@MTP, DOX/HA-EGCG, and DOX@MTP/HA-EGCG in the presence of 10 mM GSH in different buffers with varying pH values.

the MTP structure. The results showed that DOX@MTP, DOX/HA-EGCG, and MTP/HA-EGCG have great thermal stability up to 200 °C. MTP/HA-EGCG and DOX@MTP/HA-EGCG were excellently resolubilized after lyophilization (Figure S8), providing a strong foundation for the preparation, storage, and industrial use of the nanoreactors.

In vitro ·OH assay

MB was used as an indicator to evaluate the generation of ·OH, which decreased MB absorbance. The date of Fig. 1C indicated that the intensity of the spectra of MB treated with $FeCl_3$, MTP, MTP/HA-EGCG, and DOX@MTP/HA-EGCG was significantly decreased compared with that of MB incubated with H_2O_2 alone. The absorbance at 550–700 nm of MB treated with MTP was lower than that of MB treated with $FeCl_3$ group. The catalytic efficiency of Fe^{3+} is lower than that of Fe^{2+}, thus, many efforts have been explored to accelerate Fe^{3+}/Fe^{2+} conversion to enhance Fenton reaction. Phenol, as a reductive substance, can reduce Fe^{3+} into Fe^{2+} for the high effect of Fenton reaction for CDT [14]. So, EGCG can continuously supply Fe^{2+} to generate additional ·OH caused the MB decolorization. The absorbance of MTP/HA-EGCG and DOX@MTP/HA-EGCG prepared by introduction of the HA-EGCG carrier did not change compared with that of MTP, indicating that HA-EGCG did not influence the efficiency of the Fenton reaction of MTP. Because of acid responsiveness of MTP, MTP/HA-EGCG, and DOX@MTP/HA-EGCG, iron ions were released faster in a low pH environment, and the efficiency of the Fenton reaction was enhanced, resulting in an increase in the degradation rate of MB.

In vitro release behavior of DOX

The specific microenvironment of tumor cells provides the new strategy for cancer therapy. Therefore, we designed the nanoreactor to respond to both acid and GSH to accelerate drug release in tumor tissues. The DOX release profiles from DOX@MTP, DOX/HA-EGCG, and DOX@MTP/HA-EGCG were analyzed using a dialysis method (Fig. 1D). Changes in pH induced, various MTP states, including monocomplexes (pH < 2), bis-complexes (3 < pH < 6), and tris-complexes (pH > 7) [41,42]. Thus, after 124 h, the cumulative release of DOX in a buffer at pH 5.4 was higher than that in PBS at pH 7.4. Disulfide bonds, as dynamic bonds, can be cleaved by reductive substance (for example, GSH). Thus, the GSH sensitivity of DOX/HA-EGCG and DOX@MTP/HA-EGCG was measured owing to the presence of disulfide bonds in the HA-EGCG structure. In the presence of 10 mM GSH in a buffer, the cumulative release values of DOX in the DOX/HA-EGCG and DOX@MTP/HA-EGCG groups were 51.5 ± 1.2% (pH 5.4) and 39.5 ± 0.9% (pH 7.4) and 60.1 ± 1.3% (pH 5.4) and 48.3 ± 1.6% (pH 7.4), respectively. These values were higher than those in the DOX/HA-EGCG and DOX@MTP/HA-EGCG groups in the absence of GSH. Thus, drug release from DOX@MTP/HA-EGCG depended on two factors, acidic pH response of MTP and the response of the HA-EGCG layer to GSH. Lower release profile in a buffer at pH 7.4 buffer indicated that DOX leakage in the circulation can be reduced. Taken together, the combination of GSH- and pH-triggered disassembly of the nanoreactor could make full use of the acidic tumor microenvironment and intracellular redox homeostasis to specific release drug, resulting in maximum therapeutic effects.

Investigation of cell uptake mechanism

Previous studies reported that HA have the high bind affinity for CD44 receptor to accelerate the internalization into tumor cells [21]. Thus, CD44 expression in GL261 cells was determined by CLSM and flow cytometry (Figure S9). The results confirmed that the CD44 receptor is overexpressed in GL261 cells, indicating that

GL261 cells may have high affinity binding for HA. Cellular uptake of DOX was evaluated in GL261 cells after treatment with DOX, DOX/HA-EGCG, and DOX@MTP/HA-EGCG for 1, 2, and 4 h by CLSM (Fig. 2A) and flow cytometry (Fig. 2B and Figure S10). The fluorescence signal intensity in the DOX group was higher than that in the DOX/HA-EGCG and DOX@MTP/HA-EGCG groups at every time point apparently due to passive diffusion of DOX. At extended incubation time, the fluorescence signal intensity in the DOX/HA-EGCG and DOX@MTP/HA-EGCG groups were increased, suggesting that uptake of the nanoreactors by GL261 cells was time-dependent. Subsequently, to investigate the cellular uptake mechanism of DOX@MTP/HA-EGCG in GL261 cells, a competitive inhibition experiment was performed in the presence of free HA (10 mg/mL). As illustrated in Fig. 3A(a), the nanoreactor level in the cell was decreased in the presence of free HA. The fluorescence intensity of DOX was weaker than that of the group without free HA by flow cytometry (Fig. 3A(b)), suggesting that DOX@MTP/HA-EGCG entered the cells via an CD44-mediated endocytosis.

In addition to the CD44-mediated pathway, we investigated other potential mechanisms by which DOX@MTP/HA-EGCG may enter the cells. Various inhibitors of endocytosis, including dynasore (dynamin), CPZ (clathrin), M-β-CD (caveolae), and EIPA (micropinocytosis), were applied to GL261 cells [43]. As shown in Fig. 3B and 3C, preincubation of GL261 cells with specific inhibitors CPZ and M-β-CD affected endocytosis. These inhibitors reduced cellular uptake capability, suggesting that caveolae- and clathrin-mediated endocytosis play an important role in internalization of DOX@MTP/HA-EGCG. However, high intensity of the signal was retained in GL261 cells pretreated with dynasore and the fluorescence signal intensity was slightly decreased after the addition of EIPA, indicating that dynamin and micropinocytosis have a weak effect on nanoreactor endocytosis. Overall, the nanoreactors were efficiently internalized into GL261 cells by CD44 receptor-mediated endocytosis dependent on clathrin and caveolae.

Colocalization of DOX@MTP/HA-EGCG

After internalization of the nanoreactor in the tumor cells, acidic lysosomal medium and lysosomal hydrolases are expected to degrade the nanoplatform, which is the major obstacle for antitumor effects. Thus, we developed the nanoreactor. The data shown in Fig. 3D illustrate the colocalization of DOX@MTP/HA-EGCG in GL261 cells with labeled lysosomes (green). After incubation with the nanoreactor for 4 h, the red fluorescence signal of the nanoreactor predominantly overlapped with the green signal of the lysosomes, indicating that the nanoreactor was effectively internalized by GL261 cells. Prolonged incubation resulted in a gradual shift of the red fluorescence signal from the lysosomes to enter the cytoplasm, indicating that the DOX@MTP/HA-EGCG nanoreactors escaped the lysosomes. Because of a high GSH level in tumor cells, the shell of the nanoreactor dissociates to release the DOX@MTP core, and the MTP moiety of DOX@MTP readily escape lysosomes due to the "proton-sponge effect" arising from the buffering capacity [44,45]. MTP with pH-buffering capacity buffer the influx of protons to enhance osmotic rupture of lysosomes membrane.

Assay of cytotoxic and apoptotic effects of DOX@MTP/HA-EGCG

Great biocompatibility is essential for the biological application of the nanomaterials. Thus, the safety of HA-EGCG was determined by 3-(4,5-dimethyl-2-thiazolyl)-2,5-diphenyl-2H-tetrazolium bromide (MTT) assay (Figure S11). Cytotoxicity of HA-EGCG was tested in the normal L929 cell line, and the results indicated that cell viability exceeded 85% at the concentration of the agent of 1.2 mg/mL, illustrating considerable biosafety of HA-EGCG. The antitumor activity of EGCG and HA-EGCG was measured in GL261 cells. The HA-EGCG carrier was able to maintain its antitumor effect compared with that of EGCG at the same concentration (Fig. 4A). Subsequently, we detected the cytotoxicity of DOX, DOX/HA-EGCG, DOX@MTP, and DOX@MTP/HA-EGCG in GL261 cells (Fig. 4B), and the half-maximal inhibitory concentrations (IC_{50}) are displayed in Fig. 4C. DOX and DOX-loaded nanoreactors had concentration-dependent cytotoxicity in GL261 cells. Because of inefficient DOX release, the IC_{50} values of DOX/HA-EGCG, DOX@MTP, and DOX@MTP/HA-EGCG were higher than that of free DOX. The disulfide bond of HA-EGCG consumed GSH to enhance CDT; thus, DOX@MTP/HA-EGCG had a lower IC_{50} value than that of DOX@MTP. The synergistic effect of CDT and chemotherapy corresponded to lower IC_{50} values of DOX@MTP and DOX@MTP/HA-EGCG compared with that of DOX/HA-EGCG.

Cell apoptosis is one of the major mechanisms of chemotherapy-induced cell death. Thus, we evaluated apoptosis induced by MTP/HA-EGCG, DOX, DOX@MTP, DOX/HA-EGCG, and DOX@MTP/HA-EGCG nanoreactors in GL261 cells by double staining with Annexin V-FITC/7AAD (Fig. 4D). The percentages of apoptotic cells in the MTP/HA-EGCG, DOX, DOX/HA-EGCG, DOX@MTP, and DOX@MTP/HA-EGCG groups were 11.64 ± 1.49, 15.34 ± 2.38, 17.64 ± 1.03, 29.91 ± 2.12, and 38.67 ± 1.98%, respectively (Fig. 4E), suggesting that the percentage of apoptosis induced in the single chemotherapy or CDT groups was lower than that induced in the synergistic treatment groups. The expression level of cleaved caspase 3 was measured by WB (Fig. 4F). The results indicated an induction of the expression levels of apoptotic proteins and were consistent with the data of flow cytometry. After internalization by GL261 cells, DOX@MTP/HA-EGCG released DOX, Fe^{3+}, and EGCG at lower pH and high GSH levels. Due to high reduction potential, EGCG converted Fe^{3+} to Fe^{2+} to improve CDT via the Fenton reaction. Thus, the antitumor effect in the DOX@MTP/HA-EGCG group was substantially higher than that in other groups due to a combination of chemotherapy and CDT.

ROS and GSH assays

ROS play important roles in vital processes. High ROS levels can induce oxidative damage to cellular biomacromolecules, leading to cell death [46]. DCFH-DA was used as a probe to measure ROS after treatment with $FeCl_3$, MTP, and MTP/HA-EGCG (Fig. 5A). Weak green fluorescence was observed after treatment with $FeCl_3$, and a strong fluorescence signal was observed in the MTP groups, suggesting the amplification of ROS generation triggered by EGCG and Fe^{3+}. EGCG accelerate Fe^{3+}/Fe^{2+} conversion to produce more ·OH [14]. The introduction of HA-EGCG enhanced the levels of intracellular ROS by depleting GSH in the MTP/HA-EGCG group. Subsequent addition of a ROS scavenger (VC) and an iron chelator (DFO) blocked amplification effect, indicating the involvement of Fe^{3+} in ROS production.

High levels of GSH in tumor cells (1–15 mM) can scavenge ROS to maintain intracellular homeostasis, which is a major barrier for CDT. Dynamic disulfide bonds can be cleaved upon consumption of GSH to increase CDT efficiency [47]. The level of GSH was decreased by 33.3%, 41.6%, and 75.0% after incubation with HA-EGCG, MTP, and MTP/HA-EGCG, respectively, compared with that in the control group (Fig. 5B). The disulfide bond of HA-EGCG could simultaneously consume GSH to release MTP and initiate the iron ions of MTP converted GSH to GSSG [48]. Thus, a combination of disulfide bonds with MTP significantly decreased GSH levels and amplified oxidative stress.

Evaluation of in vitro BBB transcytosis

BBB is a natural defense system that prevents penetration of the drugs from cerebral vessels into the brain, resulting in poor efficacy

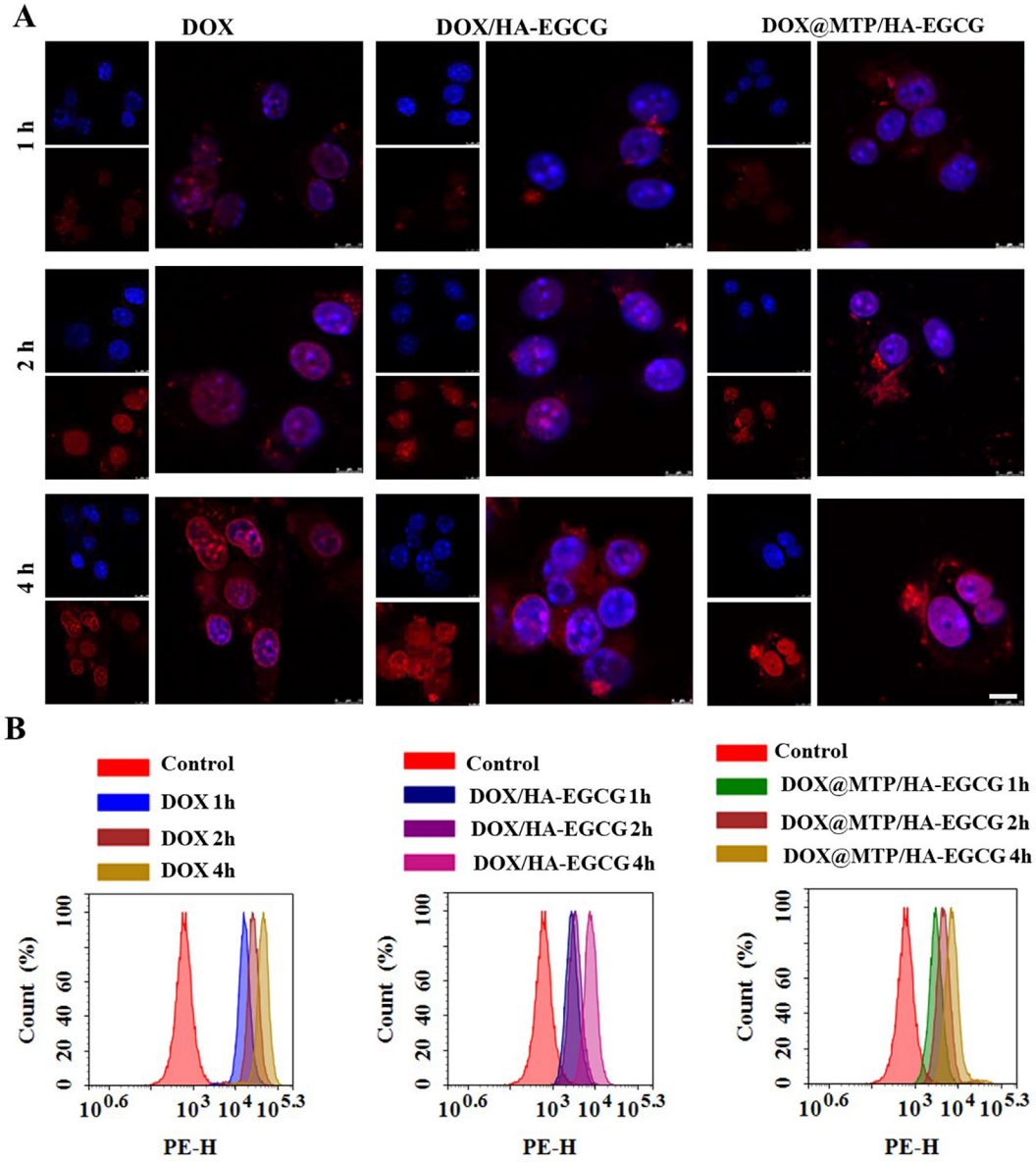

Fig. 2. Cellular uptake of DOX, DOX/HA-EGCG, and DOX@MTP/HA-EGCG NPs by CLSM (A) and quantitative analysis of the cellular uptake of DOX by flow cytometry (B). The scale bar is 10 μm.

of chemotherapy [49–51]. Due to EPR effect, the nanoreactor can penetrate through the BBB to deliver drugs. Interestingly, EGCG disrupts the BBB by breaking tight junctions between cerebrovascular endothelial cells [22,52]. Thus, an *in vitro* BBB model was developed to study the ability of DOX@MTP, DOX/HA-EGCG, and DOX@MTP/HA-EGCG to penetrate through the BBB. bEnd.3 cells were used to provide the basal membrane in the donor chamber, and GL261 cells were used in the acceptor chamber to determine the BBB transcytosis capacity of the nanoreactor. A fluorescence signal was observed after GL261 cells were incubated with DOX@MTP for 4 h (Fig. 5C), indicating that the nanoreactor can cross the BBB via the EPR and EGCG effects. After incubation with DOX/HA-EGCG and DOX@MTP/HA-EGCG, an enhanced fluorescence signal was observed in GL261 cells compared with that in DOX and DOX@MTP groups, suggesting that HA-EGCG coatings may facilitate the translocation of the nanoreactor across the bEnd.3 monolayers. Additionally, flow cytometry was used for quantitative analysis of fluorescence intensity in bEnd.3 and GL261 cells (Fig. 5D). Fluorescence signals were detected in bEnd.3 cells, indicating that the nanoreactor was internalized through the bEnd.3 monolayers. The DOX/HA-EGCG and DOX@MTP/HA-EGCG groups of GL261 cells had higher florescence intensity than that in DOX and DOX@MTP groups, corroborating qualitative results described above.

In vivo biodistribution of the nanoreactor

To explore the targeting and accumulation capacity of the RB@MTP/HA-EGCG nanoreactor, the *in vivo* biodistribution of RB, RB@MTP, RB/HA-EGCG, and RB@MTP/HA-EGCG was observed in GL261 glioblastoma-bearing mice using an imaging system (Figure S12). Fluorescence signals at a brain site were detected in the four groups 2 h after intravenous injection. The signals in the RB@MTP, RB/HA-EGCG, and RB@MTP/HA-EGCG groups were stronger than those in the RB group. Extended time of administration resulted in enhance fluorescence intensity in the RB/HA-EGCG and RB@MTP/HA-EGCG groups in the brain, and the signal in the RB group disappeared because of rapid clearance. The nanoreactors

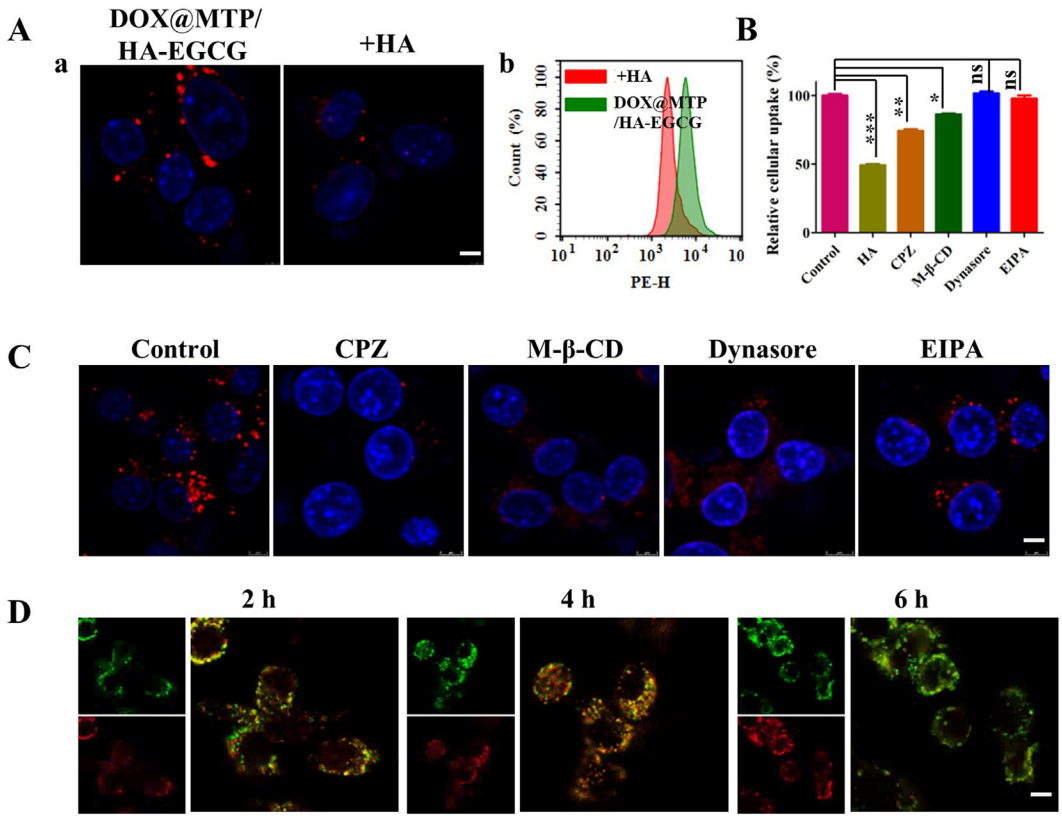

Fig. 3. Internalization behavior of DOX@MTP/HA-EGCG NPs. (A) Confocal images (a) and flow cytometry (b) of GL261 cells incubated with DOX@MTP/HA-EGCG NPs in the absence and presence of 10 mg/mL of HA. Effects of chlorpromazine hydrochloride (CPZ), M-β-CD, dynasore, and EIPA on the endocytosis of DOX@MTP/HA-EGCG NPs by GL261 cells, as determined by flow cytometry (B) and CLSM (C). (D) Distribution of DOX@MTP/HA-EGCG NPs in lysosomes after incubation with GL261 cells for 2 h, 4 h, and 6 h. The scale bar is 5 μm. *P < 0.05, **P < 0.01, ***P < 0.001.

were able to penetrate the BBB due to the effects of EGCG and EPR. Comparison with the RB and RB@MTP groups indicated that the RB/HA-EGCG and RB@MTP/HA-EGCG groups had very strong fluorescence signals at 10 h, confirming that considerable targeting capacity of HA-EGCG enhanced brain distribution of the nanoreactors *in vivo*. The signal gradually decreased due to elimination with the flow of blood. After administration for 24 h, a fluorescence signal was observed in the RB/HA-EGCG and RB@MTP/HA-EGCG groups, suggesting that the nanoreactor with the HA-EGCG coating was able to selectively home to the tumor. The brain and other organs were collected after intravenous injection for 24 h to assess the distribution (Fig. 6A). *Ex vivo* imaging revealed a fluorescence signal of RB in the brain. Additionally, liver and kidney cells expressing integrin receptors recruited nanoreactors. Liver is the major metabolic organ that also accumulated the nanoreactors. To determine the distribution of the nanoreactors in the tumors, frozen sections of the brain were stained with DAPI and the results were consistent with the data of *in vivo* imaging (Fig. 6B).

In vivo tumor therapy

Orthotopic GL261-Luci-bearing C57BL/6 mice were used to evaluate the antiglioblastoma efficacy of DOX-based formulations. GL261 cells were modified to express the luciferase enzyme, and *in vivo* imaging was used to determine tumor growth (Fig. 7A). The data of IVIS spectroscopy indicated that the tumors treated with MTP/HA-EGCG, DOX, and DOX/HA-EGCG showed a moderate growth inhibition effect due to the CDT and chemotherapy, respectively. It is worth noting that the treatment of DOX@MTP and DOX@MTP/HA-EGCG could significantly inhibit the tumor growth via CDT and chemotherapy.

Additionally, we detected the antitumor effects of various formulations after intravenous administration in a survival study (Fig. 7B). GL261 glioblastoma-bearing mice treated with MTP/HA-EGCG had a moderately prolonged median survival time (from 21 to 28 days) compared with that in the NS group. The median survival times of glioblastoma-bearing mice treated with DOX and DOX/HA-EGCG were 30 days and 35 days, respectively. Antiglioblastoma effect in the DOX/HA-EGCG group was better than in the DOX group treated with the same dose of DOX primarily because the HA-EGCG coating might penetrate through the BBB and deliver higher amounts of DOX to the tumors via CD44-mediated active targeting. Longer survival times (43 days and 60 days) were detected in the DOX@MTP and DOX@MTP/HA-EGCG groups, respectively.

Improved therapeutic performance in the DOX@MTP and DOX@MTP/HA-EGCG groups was likely due to CDT-enhanced chemotherapy, as suggested by the data of *in vivo* imaging. The HA-EGCG coating caused CD44-mediated active targeting and amplification of oxidative stress; hence, survival time was extended in the DOX@MTP/HA-EGCG group compared with that in the DOX@MTP group. Additionally, the body weight of GL261-bearing mice after treatment with various formulations was significantly different (Figure S13). These differences can be explained by the influence of nerves suppressed by the tumor on appetite at later treatment points.

Brain tumors were imaged by MRI after the treatments to observe the therapeutic outcomes (Fig. 7D(a) and Figure S14). After treatment with various formulations, the tumor volumes of

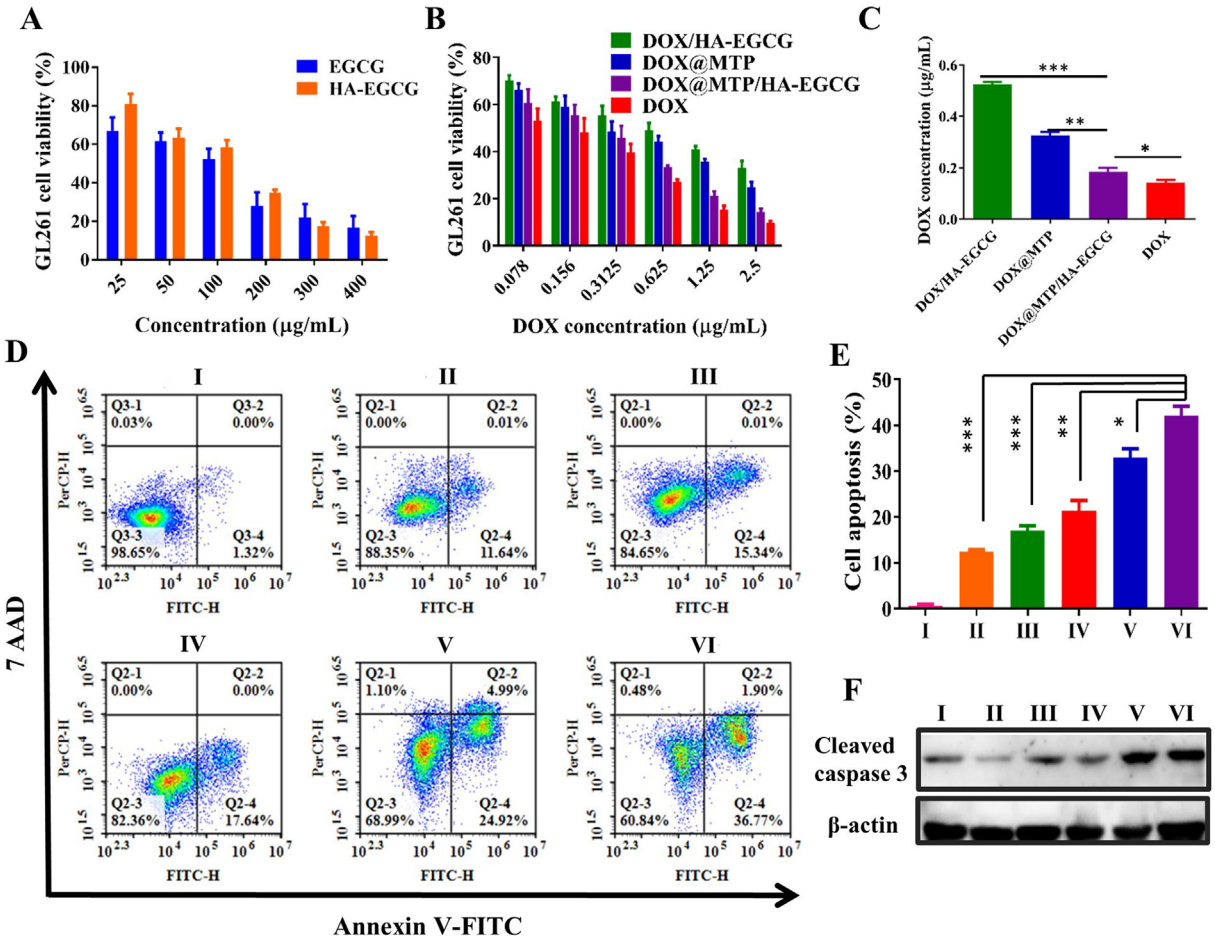

Fig. 4. Therapeutic efficacy of DOX@MTP/HA-EGCG NPs in GL261 cells via chemotherapy and CDT. (A) Cytotoxicity of GL261 cells treated with EGCG and HA-EGCG conjugates, as determined by MTT assay. (B) Cytotoxicity and IC_{50} (C) of GL261 cells treated with DOX, DOX/HA-EGCG, DOX@MTP, and DOX@MTP/HA-EGCG NPs. (D, E) Apoptosis of GL261 cells after treatment for 24 h, as measured by flow cytometry using the Annexin V-FITC/7AAD kit. (F) Expression of caspase 3 protein, as determined by Western blot analysis in GL261 cells after treatment with MTP/HA-EGCG, DOX, DOX@MTP, DOX/HA-EGCG, and DOX@MTP/HA-EGCG for 24 h. Untreated cells served as the control. I: Control; II: MTP/HA-EGCG; III: DOX; IV: DOX/HA-EGCG; V: DOX@MTP; VI: DOX@MTP/HA-EGCG.

DOX@MTP and DOX@MTP/HA-EGCG groups showed significantly smaller than that of other groups (Fig. 7C). The results were consistent with the data of IVIS spectroscopy and survival time analysis. Considerably enhanced tumor necrosis or apoptosis were detected in the DOX@MTP/HA-EGCG group compared with those in other groups (Fig. 7D(b)). Immunohistochemical staining for Ki67 (Fig. 8A) and CD31 (Fig. 8B) of the tumor sections was used to evaluate tumor cell proliferation and angiogenesis. The results indicated that Ki67 expression was significantly decreased and angiogenesis was inhibited in the DOX@MTP/HA-EGCG group. Off-target toxicity has been highly valued when employing the nanoparticles for clinical translation. Thus, the *in vivo* biosafety assessment is very necessary. The histological analysis of the major organs revealed that no inflammation nor lesions after treated with the nanoreactor, which is similar to that observed in the control group, suggesting that the DOX-loaded nanoreactors display an excellent biosafety (Figure S15).

Conclusion

In summary, we successfully designed a natural EGCG derivative (HA-EGCG) and developed a DOX@MTP/HA-EGCG nanoreactor based on MTP to improve the active targeting of glioblastoma via CDT-enhanced chemotherapy. Acid/GSH-triggered release from DOX@MTP/HA-EGCG was able to achieve tumor-specific payload delivery and ROS generation. The results obtained an *in vitro* BBB model indicated that DOX@MTP/HA-EGCG penetrated the BBB and delivered the drugs to brain tumors. After cellular internalization via the CD44 receptor, the nanoreactors escaped from the lysosomes to promote sustained release of DOX, Fe^{3+}, and EGCG, to achieve chemotherapeutic effects and CDT. *In vivo* distribution data confirmed that the nanoreactors with HA-EGCG coating selectively targeted brain glioblastoma via the CD44 receptor and preferentially accumulated in the tumor tissues over an extended period of time. DOX@MTP/HA-EGCG inhibited tumor growth and prolonged the survival time of tumor-bearing mice because of the effects of CDT-enhanced chemotherapy. Thus, the nanoreactors can be used for treatment of glioblastoma by CDT-enhanced chemotherapy. However, future investigations are necessary to analyze the effect of the nanoreactors on normal cells and in animal trials for large-scale applications.

We expect that multifunctional nanoreactors are needed to provide new possibilities for potential clinical translation of CDT-enhanced chemotherapy.

Compliance with Ethics Requirements

All Institutional and National Guidelines for the care and use of animals (fisheries) were followed.

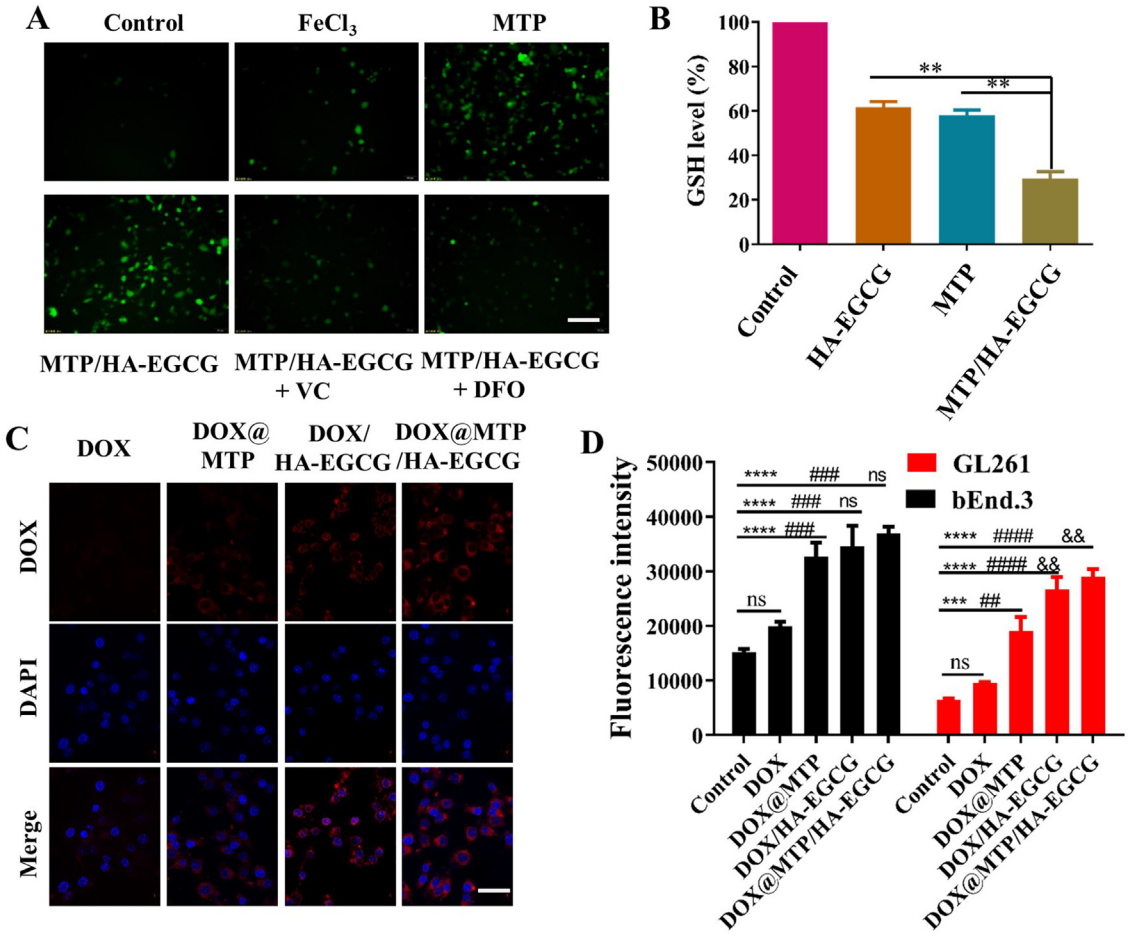

Fig. 5. (A) CLSM images of GL261 cells stained with DCF after treatment with $FeCl_3$, MTP, MTP/HA-EGCG, MTP/HA-EGCG with VC and DFO. Green fluorescence indicates the ROS level. The scale bar is 50 μm. (B) Changes in the intracellular GSH levels after treatment with HA-EGCG, MTP, and MTP/HA-EGCG. (C) Intracellular distribution of DOX in GL261 cells after transportation across the BBB. (D) Quantification of DOX distribution in the Transwell chamber after incubation with different DOX formulations. $^{**}p < 0.01$, $^{***}p < 0.001$, $^{****}p < 0.0001$; (*) represent Control vs DOX, DOX@MTP, DOX/HA-EGCG, and DOX@MTP/HA-EGCG groups; (#) represent DOX vs DOX@MTP, DOX/HA-EGCG, and DOX@MTP/HA-EGCG groups, (&) represent DOX@MTP vs DOX/HA-EGCG and DOX@MTP/HA-EGCG groups. The scale bar is 20 μm.

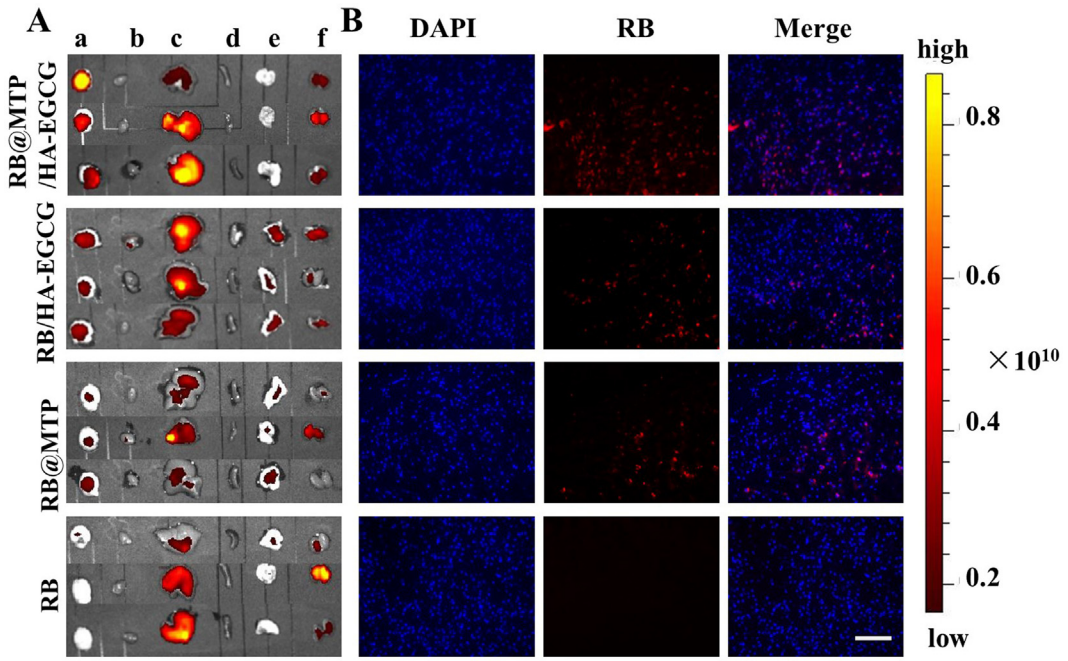

Fig. 6. In vivo tumor-targeting effects. (A) Representative fluorescence images of the brain (a), heart (b), liver (c), spleen (d), lung (e), and kidney (f) obtained after 24 h. (B) Frozen brain sections excised after 24 h and examined by CLSM. The scale bar is 50 μm.

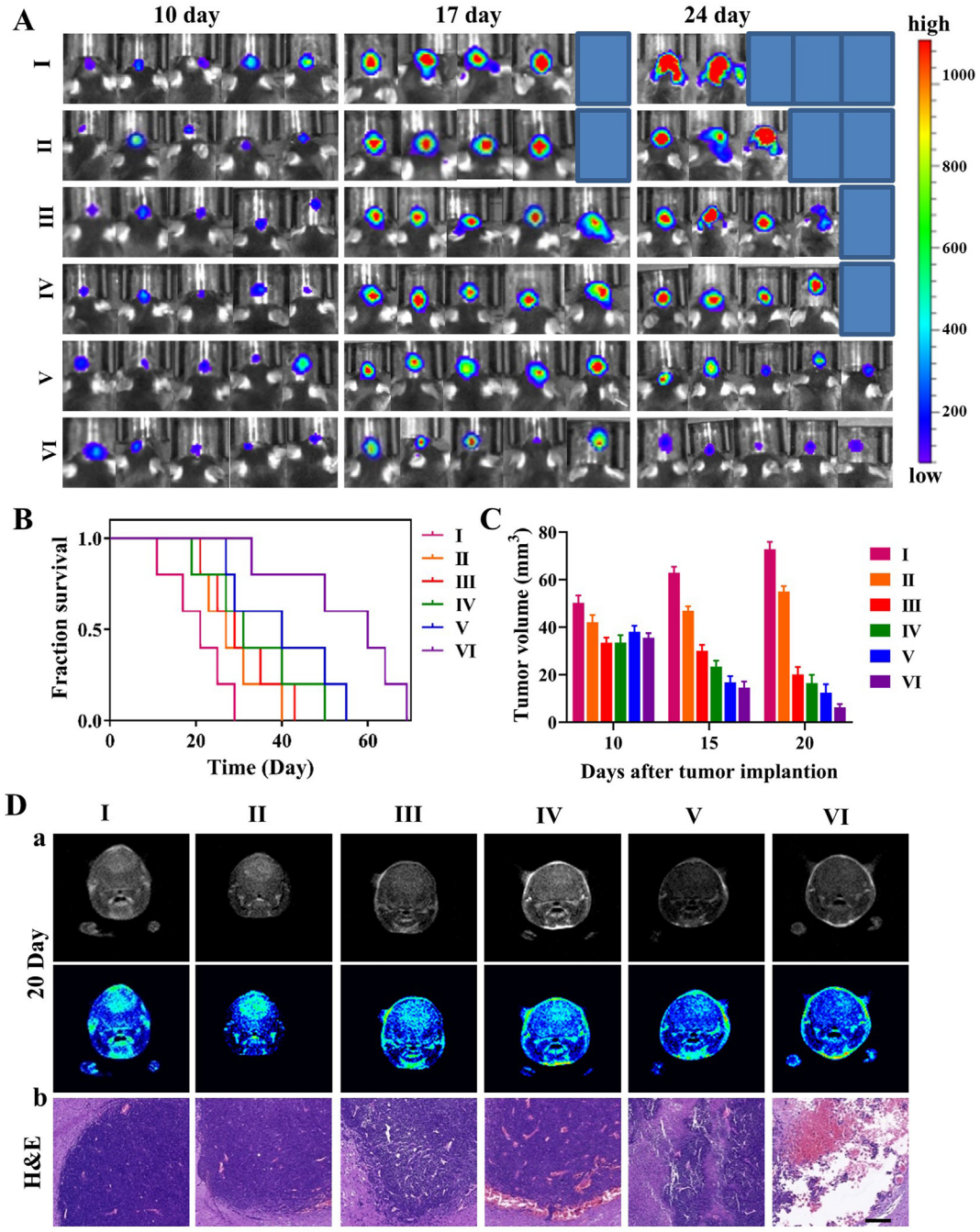

Fig. 7. In vivo antitumor efficacy of DOX@MTP/HA-EGCG NPs. (A) Bioluminescence images of C57 mice bearing orthotopic GL261-Luc glioma with different treatments (n = 5). (B) Kaplan-Meier survival curve of the mice per group. (C) The mean tumor volume using MRI at specific time after treatment with different formulations. (D) Monitoring tumor growth inhibition in GL261-bearing mice with MRI (a) after the first 20 days of treatment. (b) H&E-stained images of brain sections after treatment for 20 days with NS, MTP/HA-EGCG, DOX, DOX/HA-EGCG, DOX@MTP, and DOX@MTP/HA-EGCG NPs (DOX: 2.5 mg/kg). The scale bar is 50 μm. I: Control; II: MTP/HA-EGCG; III: DOX; IV: DOX/HA-EGCG; V: DOX@MTP; VI: DOX@MTP/HA-EGCG.

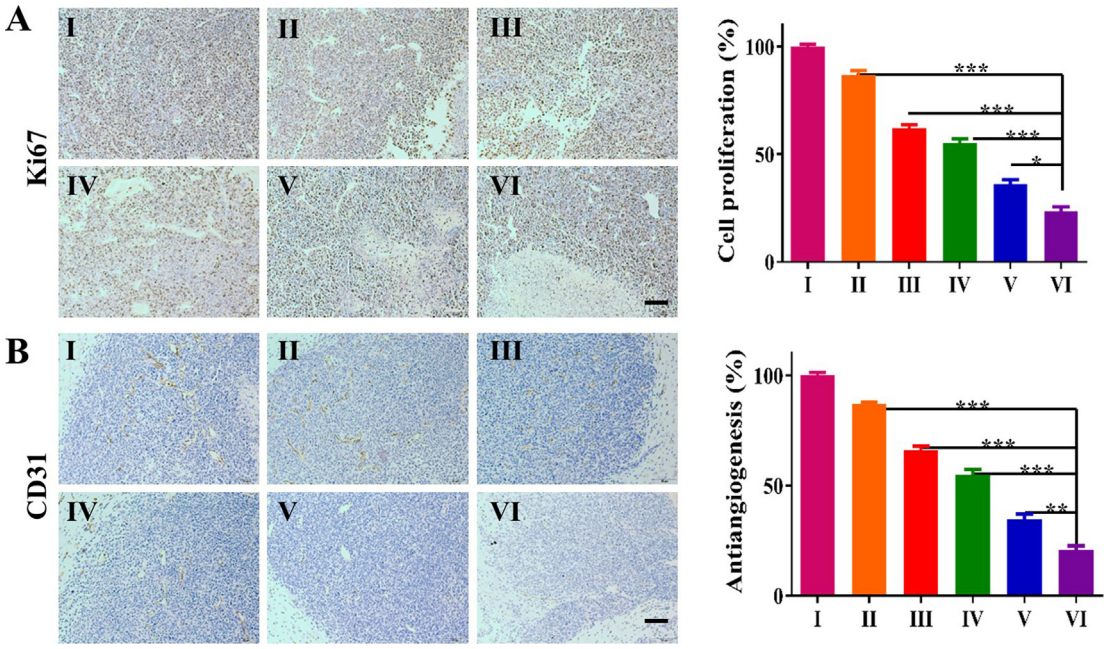

Fig. 8. Immunohistochemical staining of (A) Ki67 and (B) CD31 in mouse brains after treatment with NS, MTP/HA-EGCG, DOX, DOX/HA-EGCG, DOX@MTP, and DOX@MTP/HA-EGCG NPs for 20 days. The scale bar is 50 μm. *P < 0.05, **P < 0.01, ***P < 0.001. I: Control; II: MTP/HA-EGCG; III: DOX; IV: DOX/HA-EGCG; V: DOX@MTP; VI: DOX@MTP/HA-EGCG.

CRediT authorship contribution statement

Min Mu: Investigation, Methodology, Data curation, Writing – original draft. **Haifeng Chen:** Methodology. **Rangrang Fan:** Methodology, Formal analysis. **Yuelong Wang:** Software, Data curation. **Xin Tang:** Investigation, Methodology. **Lan Mei:** Investigation, Methodology. **Na Zhao:** Data curation. **Bingwen Zou:** Supervision. **Aiping Tong:** Supervision. **Jianguo Xu:** Resources. **Bo Han:** Validation. **Gang Guo:** Conceptualization, Funding acquisition, Writing – review & editing.

Declaration of Competing Interest

The authors declare that they have no known competing financial interests or personal relationships that could have appeared to influence the work reported in this paper.

Acknowledgments

This work was financially supported by National Natural Sciences Foundation of China (31971308, 81960769 and U1903211), National S&T Major Project (2019ZX09301-147), Sichuan Science and Technology Program (2019YFG0265), Luzhou Science and Technology Plan (2018CDLZ-10).

Appendix A. Supplementary material

Supplementary data to this article can be found online at https://doi.org/10.1016/j.jare.2021.07.010.

References

[1] Chen J, Li Y, Yu TS, McKay RM, Burns DK, Kernie SG, et al. Nature 2012;488:522–6.
[2] Kuang J, Song W, Yin J, Zeng X, Han S, Zhao Y-P, et al. Adv. Funct. Mater. 2018;28:1800025.
[3] Weller M, Wick W, Aldape K, Brada M, Berger M, Pfister SM, et al. Nature reviews. Nat. Rev. Dis. Primers 2015;1:15017.
[4] Galstyan A, Markman JL, Shatalova ES, Chiechi A, Korman AJ, Patil R, et al. Nat Commun. 2019;10:3850.
[5] Liu CH, Cao Y, Cheng YR, Wang DD, Xu TL, Su L, et al. Nat. Commun. 2020;11:1735.
[6] Chen XY, Zhang HL, Zhang M, Zhao PR, Song RX, Gong T, et al. Adv. Funct. Mater. 2019;30:1908365.
[7] Fan RR, Mei L, Gao X, Wang YL, Xiang ML, Zheng Y, et al. Adv. Sci. 2017;4:1600285.
[8] Dixon SJ, Stockwell BR. Nat. Chem. Biol. 2014;10:9–17.
[9] Shen ZY, Liu T, Li Y, Lau J, Yang Z, Fan WP, et al. ACS Nano 2018;12:11355–65.
[10] Ma YL, Zhang J, Wang Y, Chen Q, Feng ZM, Sun T. J. Adv. Res. 2019;16:135–43.
[11] Wang Z, Liu B, Sun QQ, Dong SM, Kuang Y, Dong YS, et al. ACS Appl. Mater. Interfaces 2020;12:17254–67.
[12] Zhang SC, Cao CY, Lv XY, Dai HM, Zhong ZH, Liang C, et al. Chem. Sci. 2020;11:1926–34.
[13] Chen QF, Zhou J, Chen Z, Luo Q, Xu J, Song GB, et al. ACS Appl. Mater. Interfaces 2019;11:30551–65.
[14] Zhang L, Wan SS, Li CX, Xu L, Cheng H, Zhang XZ. Nano Lett. 2018;18:7609–18.
[15] Du KK, Liu QQ, Liu M, Lv RM, He NY, Wang ZF. Nanotechnology 2019;31:015101.
[16] Liu T, Liu WL, Zhang MK, Yu WY, Gao F, Li CX, et al. ACS Nano 2018;12:12181–92.
[17] Chen ZH, Wang CH, Chen JZ, Li XD. J. Am. Chem. Soc. 2013;135:4179–82.
[18] Liu M, Liu B, Liu QQ, Du KK, Wang ZF, He NY. Coord. Chem. Rev. 2019;382:160–80.
[19] Mu M, Wang YL, Zhao SS, Li XL, Fan RR, Mei L, et al. Bio Mater. 2020;3:4128–38.
[20] Fiorica C, Mauro N, Pitarresi G, Scialabba C, Palumbo FS, Giammona G. Biomacromolecules 2017;18:1010–8.
[21] Gao S, Wang JJ, Tian R, Wang GH, Zhang LW, Li YS, et al. ACS Appl. Mater. Interfaces 2017;9:32509–19.
[22] Cano A, Ettcheto M, Chang JH, Barroso E, Espina M, Kuhne BA, et al. J. Control. Release 2019;301:62–75.
[23] Pervin M, Unno K, Nakagawa A, Takahashi Y, Iguchi K, Yamamoto H, et al. Biochem. Biophys. Rep. 2017;9:180–6.
[24] Pogacnik L, Pirc K, Palmela I, Skrt M, Kim KS, Brites D, et al. Brain Res. 2016;1651:17–26.
[25] Unno K, Pervin M, Nakagawa A, Iguchi K, Hara A, Takagaki A, et al. Mol. Nutr. Food Res. 2017;61:1700294.
[26] Huang YQ, Sun LJ, Zhang R, Hu J, Liu XF, Jiang RC, et al. Bio Mater. 2019;2:2421–34.
[27] Shan LL, Gao GZ, Wang WW, Tang W, Wang ZT, Yang Z, et al. Biomaterials 2019;210:62–9.
[28] Zhang Y, Wu KQ, Sun HL, Zhang J, Yuan JD, Zhong ZY, et al. ACS Appl. Mater. Interfaces 2018;10:1597–604.
[29] Wang XY, Wang XF, Bai X, Yan L, Liu T, Wang MZ, et al. Nano Lett. 2019;19:8–18.
[30] Fan RR, Chen CL, Hou H, Chuai D, Mu M, Liu ZY, et al. Adv. Funct. Mater. 2021;31:2009733.

[31] Liu C, Bae KH, Yamashita A, Chung JE, Kurisawa M. Biomacromolecules 2017;18:3143–55.
[32] Lee F, Lim J, Reithofer MR, Lee SS, Chung JE, Hauser CAE, et al. Polym. Chem. 2015;6:4462–72.
[33] Ouyang Q, Kou FY, Zhang NQ, Lian JT, Tu GQ, Fang ZQ. Chem. Eng. J. 2019;366:514–22.
[34] Li K, Dai Y, Chen W, Yu K, Xiao G, Richardson JJ, et al. Adv. Biosyst. 2019;3:1800241.
[35] Ren ZG, Sun SC, Sun RR, Cui GY, Hong LJ, Rao BC, et al. Adv. Mater. 2020;32: e1906024.
[36] Chung JE, Tan S, Gao SJ, Yongvongsoontorn N, Kim SH, Lee JH, et al. Nat. Nanotechnol. 2014;9:907–12.
[37] Liang K, Chung JE, Gao SJ, Yongvongsoontorn N, Kurisawa M. Adv. Mater. 2018;30:e1706963.
[38] Basha MAF. J. Adv. Res. 2018;16:55–65.
[39] Wang Y, Bai F, Luo Q, Wu ML, Song G, Zhang HM, et al. Int. J. Biol. Macromol. 2019;121:964–70.
[40] Liu P, Chen NN, Yan L, Gao F, Ji DS, Zhang SJ, et al. Carbohydr. Polym. 2019;213:17–26.
[41] Ejima H, Richardson JJ, Liang K, Best JP, van Koeverden MP, Such GK, et al. Science 2013;341:154–7.
[42] Ping Y, Guo JL, Ejima H, Chen X, Richardson JJ, Sun HL, et al. Small 2015;11:2032–6.
[43] Cai YB, Shen HS, Zhan J, Lin ML, Dai LH, Ren CH, et al. J. Am. Chem. Soc. 2017;139:2876–9.
[44] Chen JQ, Li JH, Zhou JJ, Lin ZX, Cavalieri F, Czuba-Wojnilowicz E, et al. ACS Nano 2019;13:11653–64.
[45] Liang HS, Zhou B, Li J, Liu XN, Deng ZY, Li B. J. Agric. Food Chem. 2018;66:6897–905.
[46] Wu SH, Hsieh CC, Hsu SC, Yao M, Hsiao JK, Wang SW, et al. J. Adv. Res. 2021;30:185–96.
[47] Bhattacharya K, Banerjee SL, Das S, Samanta S, Mandal M, Singha NK, et al. Bio Mater. 2019;2:2587–99.
[48] Liu JL, Wu M, Pan YT, Duan YK, Dong ZL, Chao Y, et al. Adv. Funct. Mater. 2020;30:1908865.
[49] Wang SS, Li CY, Qian M, Jiang HL, Shi W, Chen J, et al. Biomaterials 2017;141:29–39.
[50] Zhan CY, Lu WY. Curr. Pharm. Biotechnol. 2012;13:2380–7.
[51] Guo G, Fu SZ, Zhou LX, Liang H, Fan M, Luo F, et al. Nanoscale 2011;3:3825–32.
[52] Wei BB, Liu MY, Zhong X, Yao WF, Wei MJ. Acta Pharmacol. Sin. 2019;40:1490–500.